A dynamic model of a Hybrid Electric Propulsive System for degradation assessment

A dynamic model of a Hybrid Electric Propulsive System for degradation assessment

T Donateo, L Spada Chiodo and A Ficarella

Department of Engineering for Innovation, via per Monteroni, 73100 Lecce (IT)

ludovica.spadachiodo@unisalento.it

Abstract The present study proposes a model for the simulation of the steady-state and transient behaviors of a Hybrid Electric Propulsive System (HEPS), in presence of several forms and degrees of performance degradation. The power system, which is made of a turboshaft engine coupled with an electric power source is intended for urban air mobility applications. The proposed model encompasses the capability of modeling battery aging effects, and, consequently, updating the performance of the system with battery life. Moreover, the versatility of the proposed model makes it suitable for the analysis of the dynamic behavior of the system, for example in presence of small perturbations around predefined operational settings or following a known mission profile. In this investigation the model is applied to the test of the HEPS under different operating conditions with different degradation criteria, affecting both the thermal and the electric drive with different levels of severity. The application of the model allowed the generation of relevant information concerning the propulsive system state of health which will be processed with the employment of machine learning algorithms in an accompanying paper.

1 Introduction

During the last years, the recourse to electrification in aeronautical propulsive systems has increased together with the diffusion of new concepts of air mobility, including Urban Air Mobility (UAM). UAM is motivated by the necessity of reducing ground traffic in highly populated urban areas [1], and represents an interesting field of application for electric and hybrid propulsion technologies. The limited performance of current batteries makes all-electric solutions still unsuitable to be employed in large aviation [2]. Urban Air-Mobility vehicles, on the contrary, appear much more compatible to be equipped with electric and hybrid propulsive systems [3], because of their typical range of utilization in terms of speed, altitude, and power requirements. Hybrid Electric Propulsive Systems (HEPS) are a short-term solution with respect to all-electric configurations because of the increased range and endurance made possible by the presence of a dual power source. Compared with conventional power systems, HEPS have a better fuel economy and can improve safety in case of engine failure, since the electric power source can make possible a safe mission completion [4].

Previous works from the authors have focused on the investigation of proper energy management strategies for such systems as well as on their dynamic behavior, which highlighted the additional advantage of enhanced performance during transients with respect to the only-thermal configuration [5], as also suggested by [6].

However, to the authors' knowledge, no reference exists regarding the degradation of HEPS. The present work is aimed at filling the lack of scientific literature on this topic with the characterization of

different forms of degradation and the consequent performance decay. The importance of this study lies also in the possibility of obtaining useful sets of data to be exploited in health management techniques. In fact, degradation trajectories can be extensively obtained to build datasets which can be used to train machine learning algorithms that assess the system state of health [7] but it is quite impossible to apply such methods to HEPS because of the lack of experimental or numerical data.

The paper is structured as follows: Section 2 gives a detailed description of the developed model for the components of the HEPS. Section 3 describes the different approaches employed to simulate system degradation and shows some significant results for the purpose of outlining system performance decay; a subsection for each degradation approach is provided.

2 Reference vehicle and modeling approach

For the present investigation, a parallel Hybrid Electric Propulsion System for a vertical takeoff and landing (VTOL) aircraft for UAM is considered (Figure 1). The turboshaft is mechanically linked to two electric machines fed by a Li-ion battery pack. The advantages of parallel architectures versus series or more complex configurations for light aircraft are extensively analyzed in the scientific literature [8]. The parallel powertrain is connected to a coaxial rotor configuration. However, at the current stage, the connection between the shaft and the hybrid powertrain and the behavior of the external load (namely the rotor) has not been modeled in detail, as explained later.

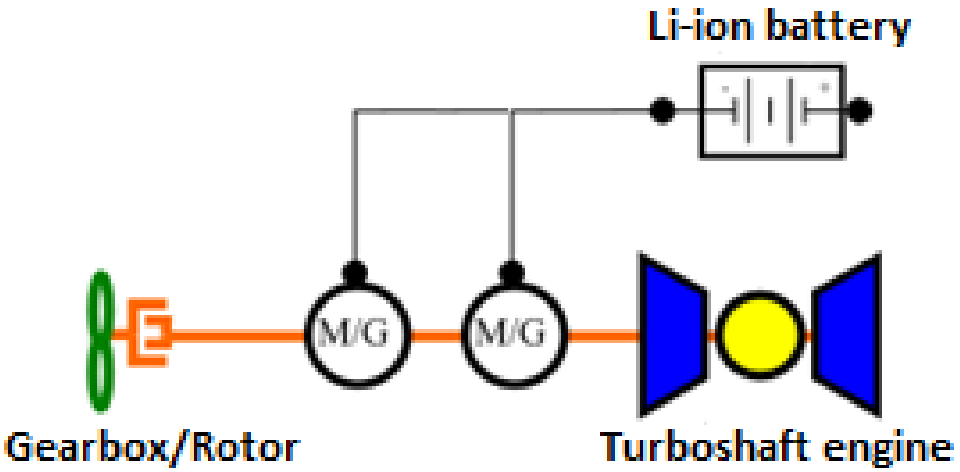

Figure 1. The parallel Hybrid Electric Propulsive System

The turboshaft (Figure 2) is a dual spool engine with a High-Pressure (HP) spool connecting the compressor and the high-pressure turbine, and a Low-Pressure (LP) spool moved by the power turbine. All rotating components (namely the compressor, the HP turbine and the LP turbine) are modeled through lookup tables which map the component pressure ratios and efficiencies as a function of the corrected mass flows and the corrected speeds. The map of each component has been obtained by scaling those of a reference turboshaft model available in GSP, to match the design requirements of the vehicle.

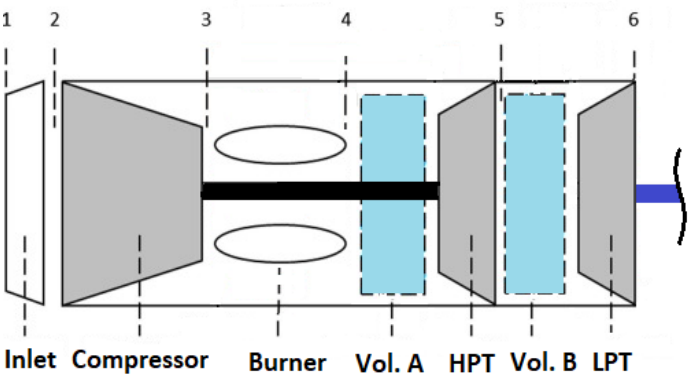

Figure 2. Scheme of the dual spool turboshaft engine

As can be seen in Figure 2, an inter-component volume (ICV) has been applied to model accumulation effects during transient phases and in particular for the flow leaving section 4 (burner exit, vol. A) and section 5 (HPT exit, vol. B). Pressure variations in such volumes are obtained by solving the following equation [9]:

$$\frac{dp}{dt} = \frac{RT}{V}\frac{dm}{dt} = \frac{RT}{V}(\dot{m}_{in}\text{-}\dot{m}_{out}) \tag{1}$$

where p and T are pressure and temperature inside the volume, V is the volume of the plenum, R the specific gas constant and the parenthesis represents the accumulation inside the volume.

The dynamics of the HP spool is modelled by applying a torque balance on the shaft:

$$\dot{N_{gg}} = \left(\frac{30}{\pi}\right)^2 \frac{1}{IN_{gg}}(P_{HPT} - P_C) \tag{2}$$

where N_{gg} and $\dot{N_{gg}}$ represent gas-generator shaft speed and acceleration, I is the corresponding shaft inertia and P_{HPT} and P_C are respectively the power output of the HP turbine and the compressor power request.

Since the rotor is not modeled in this investigation, the dynamic behavior of the LP spool is neglected at the moment and, consequently, the LP shaft speed is assumed constant. As a future development, a complete model of the rotorcraft will be considered [10].

The value of HP shaft inertia, as well as the values of inter-component volumes, have been derived from the reference GSP model. Moreover, LPT exit pressure has been mapped versus fuel flow rate with a correction to account for altitude effects.

The fuel flow rate is set by a PID controller which acts to keep LPT power output equal to shaft power demand. The controller gains have been tuned through Simulink automated tuning tool, being this aspect beyond the scope of the present work. However, a more accurate design of fuel controller is currently being investigated as further development by the authors, together with the characterization of LP spool dynamic behavior.

The electric motors are modelled through Simulink Mapped Motor block with a tabulated Torque-Speed envelope and tabulated efficiency with respect to speed and torque. The output torque tracks the torque reference command with a given time constant [11]. Being the motors connected to the same shaft as the LPT, their speed is constant too.

An in-house developed model has been used for the battery equivalent circuit [12] with voltage *V(t)* calculated as :

$$V(t) = OCV - Ri \cdot I(t) \tag{3}$$

where OCV is the open circuit voltage mapped as a function of battery SoC and R_i is the battery internal resistance, which will be updated with battery age as explained below.

The Peukert effect is included in the model in the following manner. An age-dependent Peukert coefficient *n* is considered to obtain the effective current I_{eff}:

$$I_{eff} = I \cdot \left[\frac{I}{I_{nom}}\right]^{n-1} \tag{4}$$

Moreover, a correction for battery operating temperature is included in the model to take into account its effect on battery performances as explained in [13]. Thus, battery State of Charge is calculated as:

$$SoC(t) = SoC(t_0) - 100 \cdot \int_{t_0}^{t} \frac{I_{eff}(t)}{C} \left(\frac{T_{ref}}{T}\right)^{\beta} dt \tag{5}$$

where T_{ref} is the nominal operating temperature (set at 300 K) and *T* is current operating temperature. β is the exponent which relates such temperatures to battery capacity as reported in [13].

Throughout its useful life, a lithium battery experiences an increase of internal resistance and several internal phenomena, such as loss of electrolyte and active material, which alter its behavior [14]. The main symptoms of batter aging are capacity and power fading. The former, together with an increase of the Peukert coefficient, determines energy retention, while the latter effect is ascribable mainly to the increase of the internal resistance.

To account for the ageing effect, each battery parameter *P* is expressed as a function of its number of cycles *N*, where a cycle is to be intended as a complete discharge-recharge cycle:

$$CF = \frac{P(N)}{P^0} \tag{6}$$

where *CF* is the correction factor for each battery parameter *P* (capacity, internal resistance, Peukert coefficient) and P^0 is the corresponding initial value.

Donateo and Ficarella [4] found a double exponential form for the correction factor (by interpolating experimental results from [15]:

$$CF = a \cdot exp(b \cdot N) + c \cdot exp(d \cdot N) \tag{7}$$

Conventionally the end of life of a battery is defined as number of charging/discharging cycles at which capacity reaches the 80% of its nominal value. In the model, this behavior has been implemented by means of lookup tables which map battery capacity, Peukert coefficient and internal resistance as a function of cycle number. The employed Li-ion battery has a useful life of approximately 430 cycles.

The global arrangement of the propulsive system is depicted in Figure 3. The total power request is estimated from a Pilot Interpreter block which converts a PLA input into a power command, by mapping it together with altitude and Mach effects. This power demand is given in input to a supervisory controller which determines the power split between the two power sources. The power split is expressed in terms of electric contribution *k* defined as the ratio of electric to total torque request:

$$k = \frac{Q_{EM}}{Q_{req}} \tag{8}$$

Where Q_{EM} is the torque set point for the electric machines and Q_{req} is the required torque at the rotor shaft obtained from the shaft power request and the constant speed of power shaft.

In the present study, two levels of management are used to obtain *k*. A first value of this parameter is defined by the supervisory controller according to the total power request and to the battery state of charge (SOC) and state of health (SOH). A map-based heuristic technique with fuzzy logics is used to this scope. The fuzzy logic has been developed and optimized by some of the authors in a previous work [16]. Then, the power split *k* is then corrected to improve the throttle response of the whole HEPS by means of a coordination block that adjusts *k* so that the electric machines help to counterbalance the slower dynamics of the thermal engine. This coordination effect is put into evidence in the small-perturbation analysis performed in the next section.

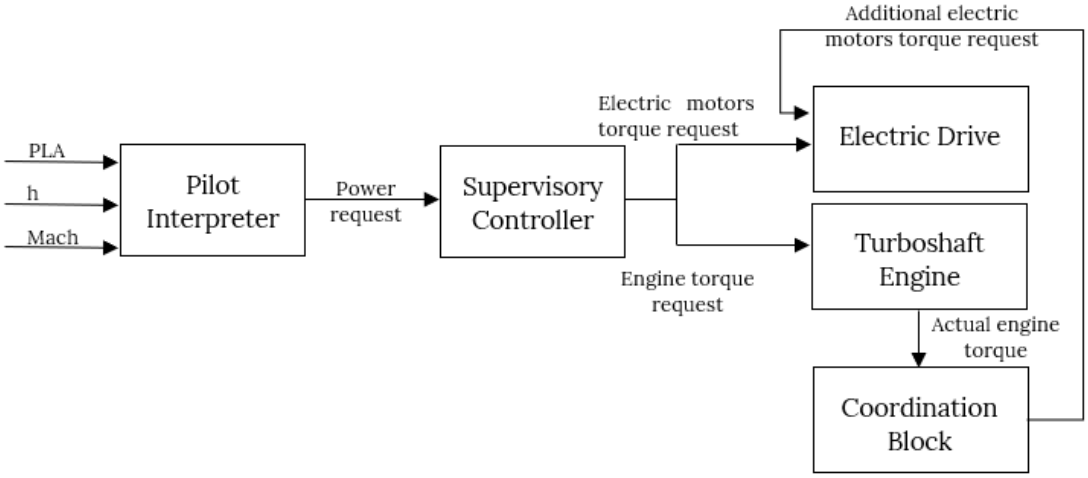

Figure 3. Scheme of the proposed HEPS

3 Degradation analysis

In this investigation the model of the HEPS and the energy management strategy explained in the previous section are used to perform the degradation tests summarized in **Table 1** and explained in the following sub-sections.

Table 1. Design of experiments for the degradation analysis

Operating conditions	Type of degradation	Degraded components
Steady-state tests	Random degradation	Burner, compressor HPT and LPT shafts electric machines battery
Small perturbations	Increasing degradation	Compressor, battery
Mission analysis	Continuous degradation	Compressor, battery

3.1 Steady-state tests

The first set of tests have been performed with reference to four operating points A-D listed in **Table 2**. The choice of these operating conditions was made by considering two different missions as shown

in Figure 4 [17]. The value of *k* and the state of charge of the battery in the four operating points were set according to the results of a previous investigation [16].

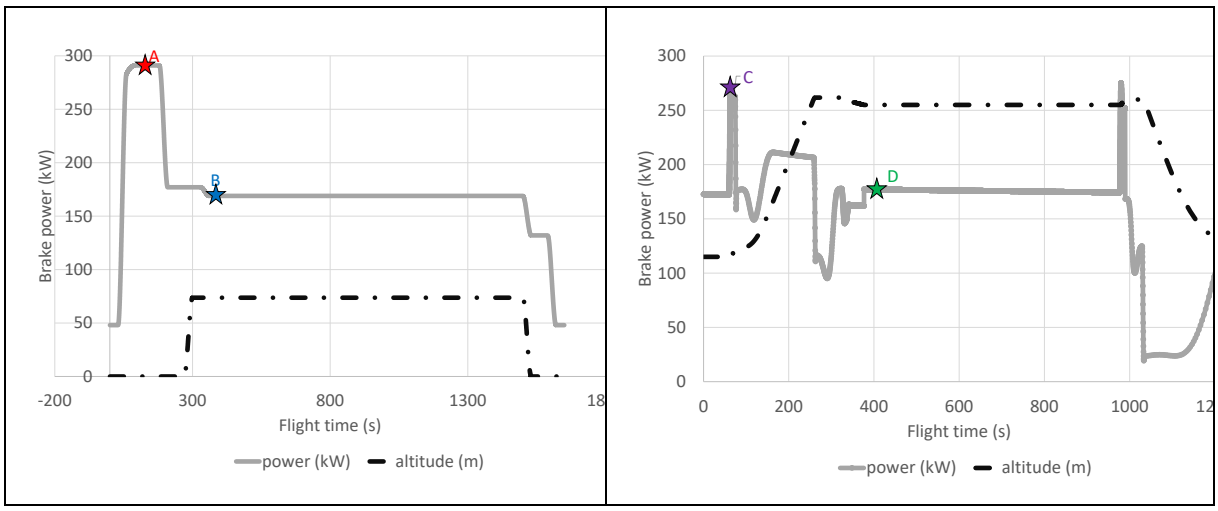

Figure 4. Choice of the operating points

Table 2. Operating conditions for the tests

	Op. point A	Op. point B	Op. point C	Op. point D
PLA (%)	65.3	50.3	68	61.5
Altitude (m)	0	492	1154	2550
True Air Speed (m/s)	30.6	30.6	4	0
Electric contribution *k*	0.4	0.7	0.47	0.6

A steady-state simulation of the four operating conditions has been carried out, with a random impact of degradation on the following parameters:

- Combustion efficiency (η_{comb}) and burner pneumatic efficiency (π_b);
- Compressor isentropic efficiency (CF $\eta_{is,c}$) and flow capacity (CF $G_{corr,c}$);
- HP and LP shaft mechanical efficiencies ($\eta_{m,HP}$, $\eta_{m,LP}$);
- Electric motor efficiency (CF η_{EM});
- Battery internal resistance (CF R_i) and Peukert coefficient (CF $n_{Peukert}$);
- Battery operating temperature ($\Delta T_{battery}$).

The maximum degradation correction was set to 0.8 of the corresponding healthy parameter, while the maximum deviation of battery operating temperature was set equal to 6°C. The model was tested with more than one hundred combinations of the random degradation coefficients for each operating condition, resulting in a huge amount of data useful to train degradation predicting machine learning algorithms [7].

The simulation results have been processed in the ModeFrontier software [18] in order to evaluate the impact of each parameter degradation on the main outputs of the model, namely the fuel flow rates, the battery residual energy, the battery voltage, and the speed of the HP shaft.

The analysis was performed with the Pearson product-moment correlation coefficient (PMCC), calculated as:

$$PMCC = \frac{cov(X,Y)}{\sigma_X \sigma_Y} = \frac{E[(X-\mu_X)(Y-\mu_Y)]}{\sigma_X \sigma_Y} \quad (9)$$

which expresses the correlation between variables X, Y given their covariance *cov(X,Y)*, defined as the expected value of the product of their deviations from their individual means μ_x and μ_y, and their standard deviations σ_x and σ_y, in the range [-1,1] [18].

The values of PMCC for one of the operating condition (Op. Point B) are reported in the correlation matrices of Figure 5. Similar results were obtained for the other operating points.

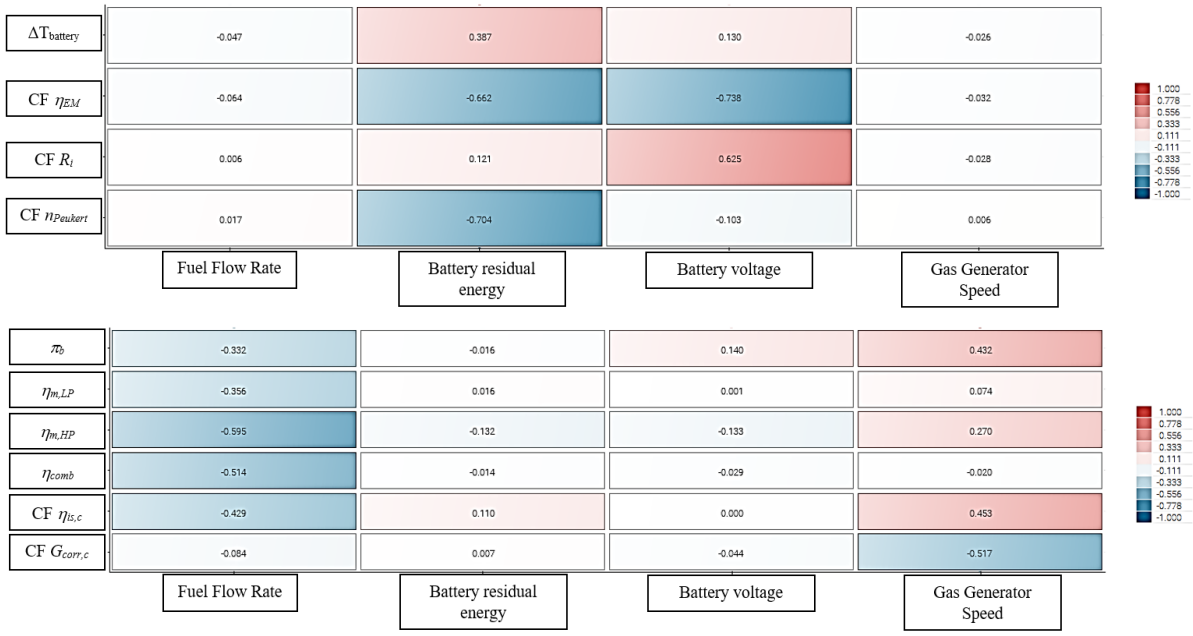

Figure 5. Correlation matrix of degradation factors and simulation outputs.

As expected, the performances of the thermal engine are not affected by electric machines degradation and vice versa, while the HP shaft mechanical efficiency appears to be the most influential parameter for fuel consumption. The negative value of the PMCC indicates that the lower the efficiency the higher the fuel consumption. The degradation of the compressor flow capacity has a huge impact on the corresponding shaft speed, again with a negative value of PMCC while the reduction of the isentropic efficiency of the compressor determines an increase in the gas generator speed. Battery residual energy appears strongly related to the Peukert coefficient and electric motor efficiency, the latter parameter being also particularly influential for battery voltage variation together with the battery internal resistance.

Among the parameters analyzed in these tests, compressor isentropic efficiency was selected to represent the degradation of the compressor in the following tests because of its high effect on both fuel flow rate and gas generator speed. The internal resistance of the battery was chosen for the battery because it is one of the parameter (together with the battery capacity) that is used in literature to define the battery state of health. Differently from the Peukert coefficient that affects the long-term behavior of the battery (see eq. (4)-(5)), the degradation of the internal resistance increases the instantaneous current to be delivered by the battery, given a certain power request as shown by eq. (3) and affects the battery discharge as well (eq. (4)-(5)).

3.2 Small perturbations

For the second set of simulations, a transient analysis has been carried out in the form of small perturbations of the reference PLA inputs of **Table 2**. The perturbation signal is shown in Figure 6. It consists of two triangular perturbations of length 0.2 s which determine an increase and a decrease of reference PLA value by an amount of 7%, and two triangular perturbations of the same amplitude but with a higher length of 6 s.

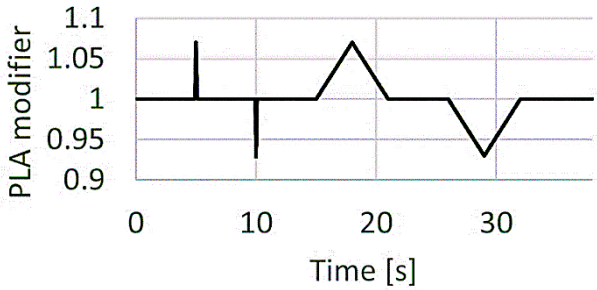

Figure 6. PLA modifier signal

For this second analysis, eleven sub-cases are provided for each operating condition. The first case simulates a healthy system. The following five cases simulate the degradation of the compressor isentropic efficiency, with a correction factor which multiplies the efficiency map output varying from 0.98 up to 0.85, to model an increasing severity of compressor damage. The last five cases model the increase of battery internal resistance, with a denominator correction factor varying from 0.98 to 0.85, too. Undegraded battery resistance is obtained from its nominal current and cell voltage.

As an example, the main simulation outputs of the first operating condition (Op. Point A) are depicted in Figure 7. As for compressor efficiency (cases 2-6), the most relevant outputs reported here are fuel flow rate and gas generator speed. The discernible behavior is that of an increasing fuel consumption with decreasing isentropic efficiency with respect to healthy condition, as expected. The compressor shaft speed decreases with decreasing compressor efficiency as already pointed out in the steady-state analysis. As for battery degradation (cases 7-11), a clear decrease of the pack voltage can be evinced, together with a slight residual energy reduction. Note that this case describes an arbitrary battery degradation, refer to Section 3.3 for a more detailed characterization of battery aging.

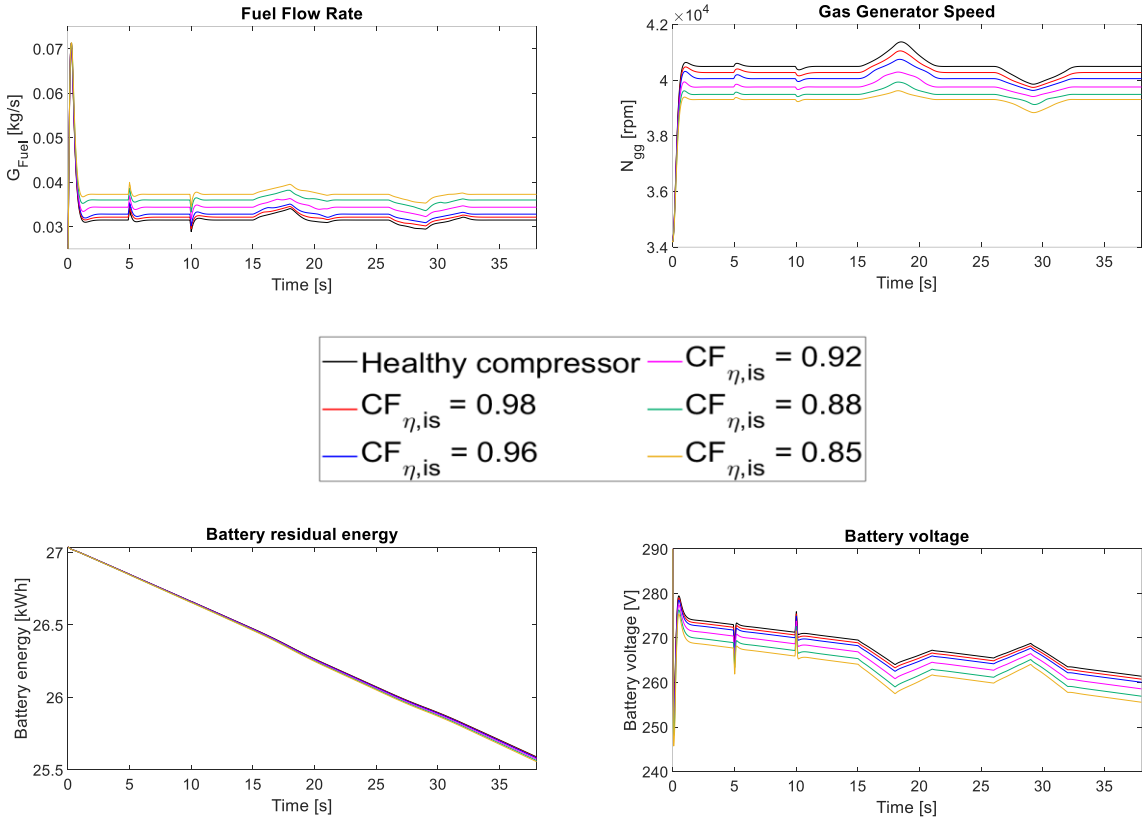

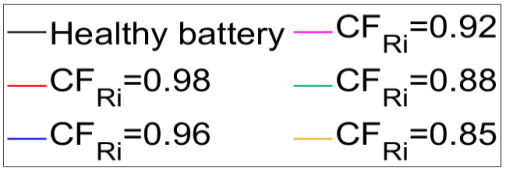

Figure 7. Results of the small perturbation analysis

3.3 Mission analysis

A whole mission has been considered for this analysis (Figure 8) and a gradual degradation of the compressor and the battery has been set. In particular, the battery age (in terms of charging/discharging cycles) was increased from 1 to 401 with a step of 100. Meanwhile, the compressor was linearly degraded in its isentropic efficiency and flow capacity. A linear correction factor has been adopted, varying from 1 (1st cycle) to 0.85 (401st cycle).

A realistic mission profile has been used for the simulations, as depicted in **Figure 8**.

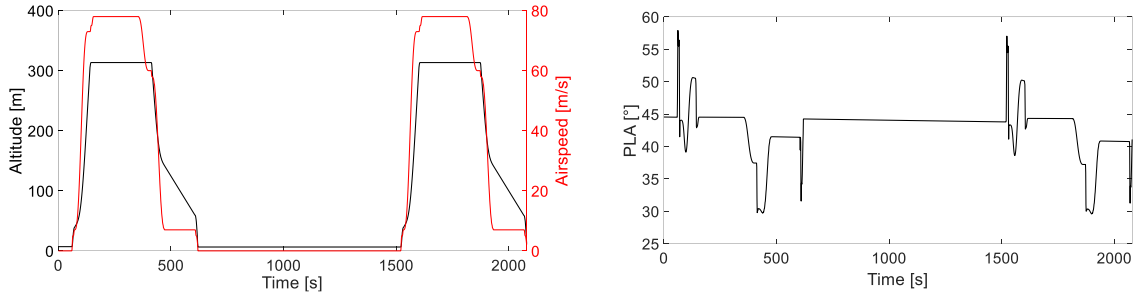

Figure 8. Mission profile.

In this case, the electric contribution has not been set arbitrarily, but was defined by the fuzzy logic supervisory controller [16], which takes into account shaft power request together with battery SoC and SoH.

The main mission simulation outputs are depicted in Figure 9, with the cumulative fuel consumption instead of the instantaneous fuel flow rate.

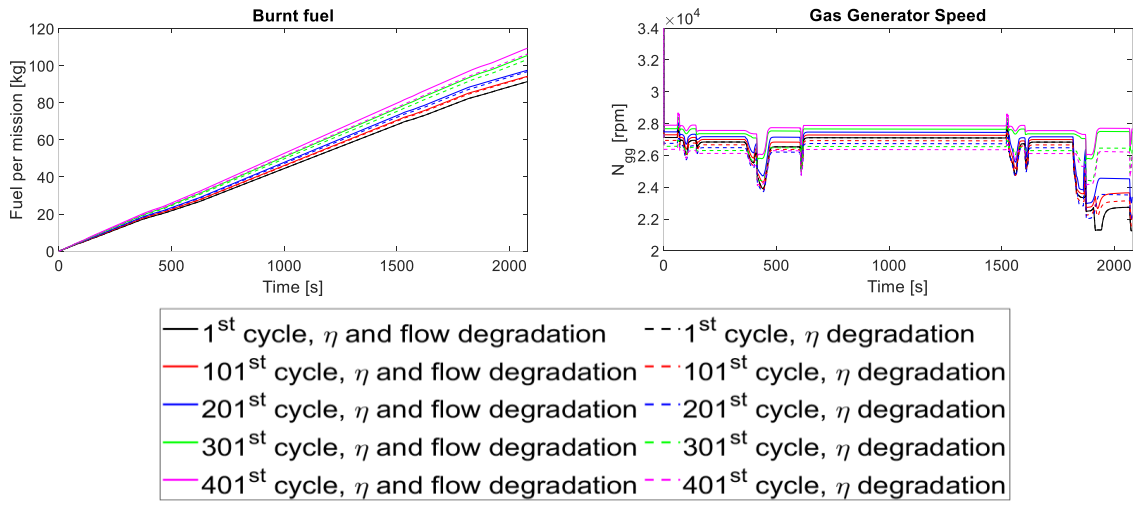

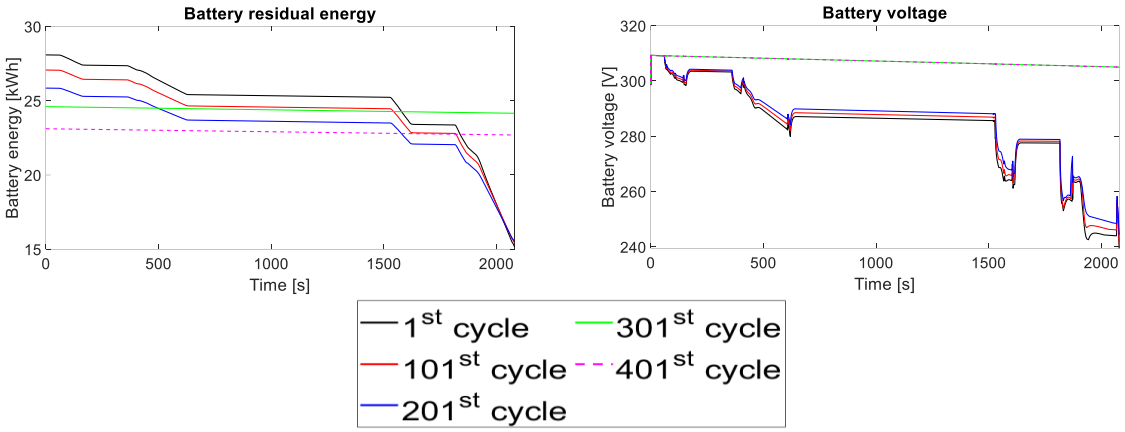

Figure 9. Results of the mission analysis with battery aging and linear compressor degradation.

The degradation of both isentropic efficiency and flow capacity of the compressor, together with worsening fuel economy, obviously alters the compressor operating points during the mission, determining a higher rotational speed with respect to the case of η_{is} deterioration only.

However, the increase in fuel consumption is determined not only by the compressor performance decay, but also from the energy management set by the supervisory controller, which excludes electric machines from power generation when the battery becomes too aged, on the basis of its established rules. This aspect is clearly visible from residual energy and voltage plots, so the adaptation of the energetic strategy to battery aging has to be always kept in mind when evaluating system degradation in this case.

4 Conclusion

The present study introduces the subject of degradation in a Hybrid Electric Propulsive System through the development of a versatile model which allows the degradation trends to be easily and extensively obtained. In this investigation, the methodology was applied to a parallel hybrid aerial vehicle for Urban Air Mobility. The powertrain consists of a parallel hybrid electric configuration where a turboshaft engine is coupled with two electric motors fed by a Li-ion battery.

The authors applied increasing degradation to compressor and battery performance parameters to observe the behavior of the system in steady-state conditions, in presence of small perturbations around the same and during a whole mission. The results of the analysis allowed to quantify the effect of degradation on the behavior of a hybrid electric power system.

The steady-state analysis confirmed that the performance of the thermal engine is not affected by electric machines' degradation and vice versa, while the HP shaft mechanical efficiency appears to be the most influential parameter for fuel consumption. The degradation of the compressor flow capacity has a huge impact on the corresponding shaft speed. Battery residual energy appears strongly related to the Peukert coefficient and electric motor efficiency, the latter parameter being also particularly influential for battery voltage variation together with the battery internal resistance. The application of the model to small perturbations and to a complete mission analysis furnished useful data that will be processed with the employment of machine learning algorithms for health monitoring.

Acknowledgements

This study was funded by the Italian Ministry for Education, University and Research and developed in collaboration with Aerospace Technological District (DTA) and Avio Aero within project SMEA - Diagnostic and Prognostic Methods and Sensors Development for the Health Monitoring in Aeronautic and Transport Applications.

References

[1] Urban Air Mobility - A game changer for smart cities https://uam.fev.com/ (retrieved on March 2022)
[2] Micro-hybridisation: the next frontier to electrify flight? https://www.airbus.com/en/newsroom/news/2021-09-micro-hybridisation-the-next-frontier-to-electrify-flight (retrieved on March 2022)
[3] Hill B P, De Carme D, Metcalfe M, Griffin C, Wiggins S, Metts C, Bastedo B, Patterson M and Mendonca N 2020 UAM Vision Concept of Operations (ConOps) UAM Maturity Level (UML) 4 Overview, *UAM UML-4 Vision ConOps Workshops*, NASA Headquarters
[4] Donateo T and Ficarella A 2020 A modeling approach for the effect of battery aging on the performance of a hybrid electric rotorcraft for Urban Air-Mobility *Aerospace* **7(5)** 56 https://doi.org/10.3390/aerospace7050056
[5] Donateo T, Spada Chiodo L and Ficarella A 2021 Transient behavior of a hybrid electric air-taxi *International Symposium on Sustainable Aviation* November 2021 Bangkok
[6] Wortmann G, Schmitz O and Hornung M 2014 Comparative assessment of transient characteristics of conventional and hybrid gas turbine engine *CEAS Aeronautical Journal* **5** 2 pp 209–223
[7] De Giorgi M G, Strafella L, Menga N and Ficarella A 2022 Intelligent Combined Neural Network and Kernel Principal Component Analysis Tool for Engine Health Monitoring Purposes *Aerospace* **9(3)** 118 https://doi.org/10.3390/aerospace9030118
[8] Finger D, de Vries R, Vos R, Braun C and Bil C 2020 A comparison of hybrid-electric aircraft sizing methods *AIAA Scitech 2020 Forum* 10.2514/6.2020-1006.
[9] Gaudet S R *Development of a Dynamic Modeling and Control System Design Methodology for Gas Turbines* Master of Applied Science, Department of Mechanical and Aerospace Engineering, Carleton University, 2007, Ottawa, Canada
[10] Ballin M G 1988 A high fidelity real-time simulation of a small turboshaft engine, NASA-TM-100991, NASA Ames Research Center, Moffett Field, CA, United States
[11] Mapped Motor https://www.mathworks.com/help/autoblks/ref/mappedmotor.html (retrieved on March 2022)
[12] Guzzella L and Sciarretta A 2007 *Vehicle Propulsion Systems: Introduction to Modeling and Optimization*, Springer, Berlin, Germany
[13] Hausmann A and Depcik C 2013 Expanding the Peukert equation for battery capacity modeling through inclusion of a temperature dependency *Journal of Power Sources* **235** pp 148-158. doi:https://doi.org/10.1016/j.jpowsour.2013.01.174.
[14] Han X, Lu L, Zheng Y, Feng X, Li Z, Li J and Ouyang M 2019 A review on the key issues of the lithium ion battery degradation among the whole life cycle *eTransportation* **1** 100005 https://doi.org/10.1016/j.etran.2019.100005
[15] Dubarry M and Liaw B 2009 Identify capacity fading mechanism in a commercial LiFePO4 cell *Journal of Power Sources* **194** pp 541-549
[16] Donateo T, Terragno A and Ficarella A 2021 An optimized fuzzy logic for the energy management of a hybrid electric air-taxi *76th Italian National Congress ATI* September 2021 Rome
[17] Donateo T, De Pascalis C, Strafella L and Ficarella A 2021 Off-line and On-line Optimization of the Energy Management Strategy in a Hybrid Electric Helicopter for Urban Air-Mobility *Aerospace Science and Technology* **113**
[18] modeFRONTIER User Guide 2019 ESTECO SpA, Trieste, Italy